Ocean Modelling 3 (2001) 33–50

Ocean Modelling

www.elsevier.com/locate/omodol

Stability of algebraic non-equilibrium second-order closure models

Hans Burchard [a,*], Eric Deleersnijder [b]

[a] *Institut für Meereskunde, Universität Hamburg, Troplowitzstrasse 7, D-22529 Hamburg, Germany*
[b] *Institut d' Astronomie et de Géophysique G. Lemaître, Université Catholique de Louvain, 2 Chemin du Cyclotron, B-1348 Louvain-la-Neuve, Belgium*

Received 20 June 2000; received in revised form 24 October 2000; accepted 9 November 2000

Abstract

Stability problems of algebraic non-equilibrium second-moment closure models have given rise to the so-called quasi-equilibrium versions in which turbulence equilibrium is used as an additional constraint. In this paper, we investigate reasons for the failure of the G.L. Mellor, T. Yamada [Reviews of Geophysics 20 (1982) 851] level 2.5 closure model and suggest a remedy for this. We further discuss a new non-equilibrium closure model by V.M. Canuto, A. Howard, Y. Cheng, M.S. Dubovikov (Journal of Physical Oceanography, 2000, accepted for publication) which has proven to allow for stable calculations. All models are then numerically tested with a simple wind entrainment experiment motivated by the H. Kato, O.M. Phillips [Journal of Fluid Mechanics 37 (1969) 643] laboratory experiment, with the aid of which the instability of the Mellor and Yamada (1982) and the stability of the Canuto et al. (2000) model are confirmed. The Canuto et al. (2000) model has three advantages compared to the Mellor and Yamada (1982) which are (i) the symmetry of stability functions, (ii) a higher critical Richardson number, and (iii) that the normalised shear stress increases with normalised shear for turbulence equilibrium. The latter advantage of the new model causes its high physical and numerical stability.

Keywords: Turbulence models; Boundary layer models; Ocean circulation models; Second-moment closure; Numerical methods; Stratified shear flow

1. Introduction

In their historical paper, Mellor and Yamada (1974) presented a hierarchy of turbulence closure models consisting of four levels, ranging from a rather complex Reynolds stress and heat flux

* Corresponding author. Tel.: +49-40-42838-2995; fax: +49-40-5605926.
E-mail address: burchard@ifm.uni-hamburg.de (H. Burchard).

1463-5003/01/$ - see front matter
PII: S1463-5003(00)00016-0

transport model to a fully algebraic turbulence closure model. In a following publication (Mellor and Yamada, 1982), they reviewed their models and added two important features: (i) a level 2.5 model which is fully algebraic in terms of the second moments and (ii) a length scale transport equation, which calculates the product of turbulent kinetic energy and the macro length scale. Since then, this specific model has been extensively applied, in large scale applications (see, Rosati and Miyakoda, 1988) as well as in coastal applications (Blumberg and Mellor, 1987).

However, several authors have reported serious stability problems with this approach (see Deleersnijder and Luyten, 1994 and Burchard et al., 1999). It could be shown that the specific algebraic closure for the second moments was responsible for these instabilities, since they occurred as well, when using other length scale parameterisations such as the dissipation rate equation. A solution to the problem had already been suggested by Galperin et al. (1988) without discussing the stability problem: to use the so-called quasi-equilibrium version of the closure for the second moments which can be derived from the Mellor and Yamada (1982) model by additionally assuming turbulence equilibrium only for the second-moment closure. Such quasi-equilibrium versions have since then substituted the full versions (see e.g., Kantha and Clayson, 1994; Mellor, 2001). Galperin et al. (1988) could actually show that the use of such quasi-equilibrium versions are not in contradiction to the use of a fully prognostic equation for the turbulent kinetic energy with the source terms not being in equilibrium. Therefore, the notation quasi-equilibrium is used. It should be noted that the term non-equilibrium, which we use here, does only imply that the quasi-equilibrium assumption is not made. However, in order to obtain an algebraic solution for the second moments, equilibrium assumptions have to be made for the second-moment transport equations, see Mellor and Yamada (1982). Not applying an equilibrium assumption on that level would lead to the rather complex level 4 model of Mellor and Yamada (1974). For this, see also Canuto (1994), where an equilibrium assumption is made on the level of third-order fluxes. Such models are usually computationally too expensive for geophysical applications.

Recently, Canuto et al. (2000) presented a new algebraic second-moment closure model which is not necessarily based on the turbulence equilibrium assumption. In this model, improvements are made for the parameterisation of pressure–strain correlations as they occur in the second-moment transport equations. In contrast to the original model of Mellor and Yamada (1982), in which two terms are used for the Reynolds stresses and one term for the heat flux, Canuto et al. (2000) use five and four terms, respectively. Burchard and Bolding (2000) showed that this new model is numerically stable and physically sound even for the non-equilibrium version.

The aim of this paper is to investigate by means of a simple wind entrainment experiment why the Mellor and Yamada (1982) algebraic second-moment closure is unstable, and to find remedies for these instabilities without assuming local equilibrium of turbulence. It will furthermore be discussed why the new Canuto et al. (2000) closure model allows for stable simulations although it is structurally similar to the former.

2. Model equations

For the idealistic simulations carried out in this paper, mean flow transport equations only for one momentum component u and buoyancy b are considered

$$\partial_t u - \partial_z(K_M \partial_z u) = 0, \tag{1}$$

$$\partial_t b - \partial_z(K_H \partial_z b) = 0 \tag{2}$$

with buoyancy

$$b = -g\frac{\rho - \rho_0}{\rho_0}, \tag{3}$$

where t is time and z the vertical coordinate, pointing upwards. Furthermore, ρ is actual and ρ_0 mean density.

Eddy viscosity K_M and eddy diffusivity K_H are modelled by the relations

$$K_M = qlS_M; \quad K_H = qlS_H, \tag{4}$$

where S_M and S_H are dimensionless stability functions, q the turbulent velocity scale and l the macro length scale of turbulence.

The quantities q and l are modelled here by means of the two-equation turbulence model suggested by Mellor and Yamada (1982). The transport equations used are one for the turbulent kinetic energy (TKE) $q^2/2$ and one for the product $q^2 l$

$$\partial_t\left(\frac{q^2}{2}\right) - \partial_z\left(qlS_q\partial_z\left(\frac{q^2}{2}\right)\right) = P_s + P_b - \varepsilon, \tag{5}$$

$$\partial_t(q^2 l) - \partial_z(qlS_q\partial_z(q^2 l)) = l\left[E_1 P_s + E_3 P_b - \left(1 + E_2\left(\frac{l}{L}\right)^2\right)\varepsilon\right] \tag{6}$$

with shear and buoyancy production

$$P_s = K_M S^2, \quad P_b = -K_H N^2, \tag{7}$$

where $N = (\partial_z b)^{1/2}$ is the Brunt-Väisälä frequency and $S = |\partial_z u|$ is the shear frequency and with the diagnostic length scale $L = \kappa z'$, where $\kappa = 0.4$ is the von Kármán constant, and z' the distance from the surface.

Following Galperin et al. (1988), the macro length scale is limited by the following constraint:

$$l \leqslant l_{\lim} = 0.53\frac{q}{N}. \tag{8}$$

The relation between the macro length scale l and the dissipation rate ε is given by means of the following equation:

$$l = \frac{q^3}{\beta_1 \varepsilon}. \tag{9}$$

Alternatively, a transport equation for the turbulent dissipation rate ε could be calculated as

$$\partial_t \varepsilon - \partial_z\left(ql\frac{S_M}{\sigma_\varepsilon}\partial_z\varepsilon\right) = 2\frac{\varepsilon}{q^2}(c_{e1}P_s + c_{e3}P_b - c_{e2}\varepsilon). \tag{10}$$

For the q^2–$q^2 l$ model, $S_q = 0.2$ and for the k–ε model, $S_q = S_M$ is used. The empirical parameters for the two models are given in Table 1. It should be noted that β_1 and $c_{\varepsilon 3}$ depend on the choice for the stability functions S_M and S_H (see Burchard and Bolding, 2000).

Table 1
Constants for the q^2–q^2l and the k–ε models[a]

E_1	E_2	E_3	β_1	c_{e1}	c_{e3}	c_{e3}	σ_ε
1.8	1.33	1.8	16.6/19.3	1.44	1.92	−0.4/−0.63	1.08

[a] The empirical parameter c_{e3} is chosen as $c_{e3} = -0.4$ for the Kantha and Clayson (1994) stability functions and $c_{e3} = -0.63$ for the Canuto et al. (2000) stability functions. The parameter β_1 is $\beta_1 = 16.6$ for the former and $\beta_1 = 19.3$ for the latter.

The surface boundary conditions which will be used here are

$$K_M \partial_z u = u_*^2; \quad K_H \partial_z b = 0; \quad q^2 = \beta_1^{2/3} u_*^2; \quad l = \kappa z_0; \quad \varepsilon = \frac{u_*^3}{\kappa z_0} \tag{11}$$

with the friction velocity u_* and the roughness length z_0. At the bottom, no-flux conditions for all prognostic quantities will be applied.

3. Stability functions

The stability functions S_M and S_H result from algebraic closures of the second moments, which differ from each other by the parameterisation of the pressure–strain correlations. These correlators contain the complex interaction between pressure fluctuations and velocity and density fluctuations. In the original version of Mellor and Yamada (1982), only the return-to-isotropy term for Reynolds stresses and turbulent heat fluxes and additionally the non-isotropic contribution due to shear for the Reynolds stresses are considered. The Kantha and Clayson (1994) model additionally considers production of turbulent heat flux by mean gradients and by buoyancy. The Canuto et al. (2000) finally is the most complete by additionally parameterising shear production, buoyancy production and vorticity for the Reynolds stresses and vorticity for the turbulent heat uxes. Each of these extensions increases the critical Richardson number, which is 0.19 for the Mellor and Yamada (1982) model, 0.24 for the Kantha and Clayson (1994) and 0.85 for the Canuto et al. (2000) model. A too low critical Richardson number has been made responsible by Martin (1985) for too little mixing at the base of the oceanic mixed layer. It should be noted that the eddy viscosity principle has not been used a priori for the derivation of the stability functions. Here we present in detail two sets of the stability functions, the model by Mellor and Yamada (1982) with the modifications by Kantha and Clayson (1994) (Section 3.1), and the new set of stability functions derived by Canuto et al. (2000) (Section 3.2).

3.1. Model of Mellor and Yamada (1982)

The following closure for the stability functions is derived according to Mellor and Yamada (1982) with some additions as suggested by Kantha and Clayson (1994):

$$S_M = \frac{a_0 + a_1 \tilde{G}_H}{1 + b_1 \tilde{G}_H + b_2 \tilde{G}_M + b_3 \tilde{G}_H^2 + b_4 \tilde{G}_M \tilde{G}_H}, \tag{12}$$

$$S_H = \frac{a_4 + a_5\tilde{G}_M + a_6\tilde{G}_H}{1 + b_1\tilde{G}_H + b_2\tilde{G}_M + b_3\tilde{G}_H^2 + b_4\tilde{G}_M\tilde{G}_H} \tag{13}$$

with

$$\tilde{G}_H = \begin{cases} G_H & \text{for } G_H \leqslant G_H^{\lim}, \\ G_H^{\lim}, & \text{else} \end{cases} \tag{14}$$

and

$$\tilde{G}_M = \begin{cases} G_M & \text{for } G_M \leqslant G_M^{\lim}, \\ G_M^{\lim}, & \text{else} \end{cases} \tag{15}$$

with the non-dimensional buoyancy and shear numbers

$$G_H = -\frac{l^2}{q^2}N^2, \quad G_M = \frac{l^2}{q^2}S^2. \tag{16}$$

The coefficients a_i and b_i are defined as follows:

$$\begin{aligned} a_0 &= A_1(1 - 3C_1), \\ a_1 &= 3A_1A_2(4A_1 + 3A_2(1 - C_2) - (1 - 3C_1)(B_2(1 - C_3) + 4A_1)), \\ a_4 &= A_2, \\ a_5 &= 18A_1^2A_2C_1, \\ a_6 &= -9A_1A_2^2, \\ b_1 &= -3A_2(3A_1 + B_2(1 - C_3) + 4A_1), \\ b_2 &= 6A_1^2, \\ b_3 &= 27A_1A_2^2(B_2(1 - C_3) + 4A_1), \\ b_4 &= 18A_1^2A_2(3A_2(1 - C_2) - B_2(1 - C_3)) \end{aligned} \tag{17}$$

with

$$C_1 = \frac{1}{3}\left(1 - \left(A_1B_1^{1/3}\right)^{-1} - 6A_1/B_1\right) \approx 0.08. \tag{18}$$

The empirical parameters may be found in Tables 2 and 3.

For $C_2 = C_3 = 0$, the original Mellor and Yamada (1982) stability functions are retained.

The limiting constraints suggested by Mellor and Yamada (1982) are as follows:

$$G_H^{\lim} = 0.033, \quad G_M^{\lim} = 0.825 - 25G_H. \tag{19}$$

Table 2
Empirical parameters for the Kantha and Clayson (1994) stability functions[a]

A_1	A_2	B_1	B_2	C_2	C_3
0.92	0.74	16.6	10.1	0.7	0.2

[a] The Mellor and Yamada (1982) stability functions are retained by setting $C_2 = C_3 = 0$.

Table 3
Empirical parameters for the Canuto et al. (2000) stability functions compared to the equivalent parameters derived for the Kantha and Clayson (1994) model

a_0	a_1	–	a_4	a_5	a_6	b_1	b_2	b_3	b_4	–
0.6979	−9.345	–	0.74	0.9070	−4.534	−32.23	5.08	159.96	−83.59	–
s_0	s_1	s_2	s_4	s_5	s_6	t_1	t_2	t_3	t_4	t_5
0.5168	−7.848	−0.0545	0.5412	−2.04	0.3964	−23.84	2.68	75.574	−45.48	−0.2937

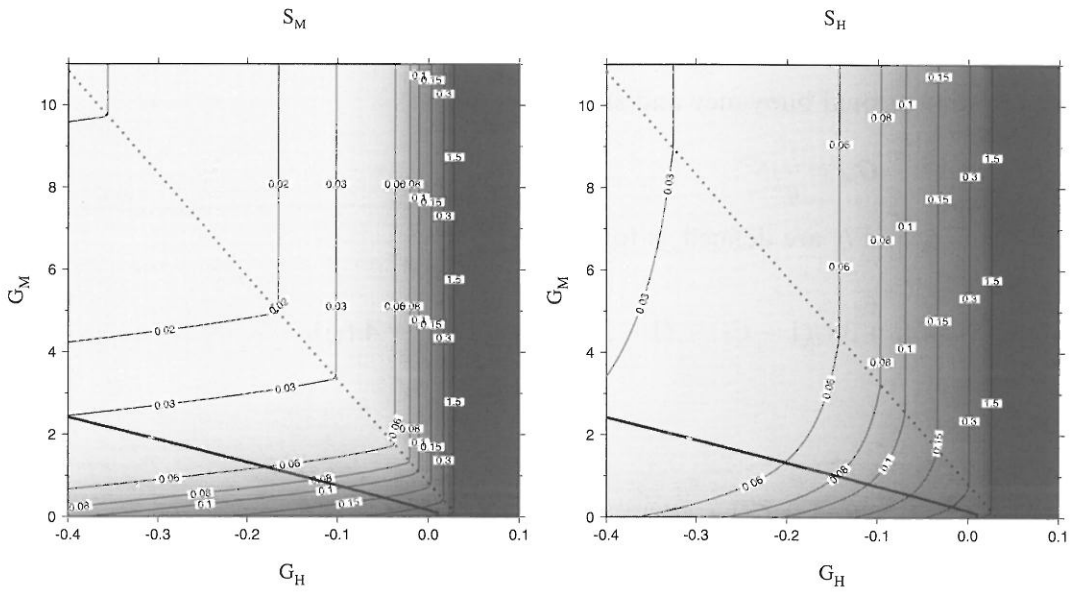

Fig. 1. The stability functions S_M and S_H as derived by Mellor and Yamada (1982). The bold lines shows the local equilibrium state (20), the dotted lines shows the constraint on G_M (19).

Kantha and Clayson (1994) use a somewhat stricter constraint for G_H, $G_H^{\lim} = 0.029$.

The Mellor and Yamada (1982) stability functions S_M and S_H are displayed in Fig. 1.

The so-called quasi-equilibrium stability functions have been introduced by Galperin et al. (1988) and are based on the assumption of local equilibrium only in the stability functions

$$P_s + P_b - \varepsilon = 0 \iff G_M = \frac{1}{\beta_1 S_M} - \frac{S_H}{S_M} G_H. \tag{20}$$

Insertion of the right-hand side of (20) into (12) and (13) leads to the quasi-equilibrium function of Galperin et al. (1988) ($C_2 = C_3 = 0$) or Kantha and Clayson (1994) ($C_2 = 0.7, C_3 = 0.2$).

3.2. Model of Canuto et al. (2000)

Although this model considers more terms for the pressure–strain correlations than the model of Mellor and Yamada (1982), they are structurally quite similar. For an intensive analysis of these new functions in comparison to others, see Burchard and Bolding (2000).

$$S_M = \frac{s_0 + s_1\tilde{G}_H + s_2\tilde{G}_M}{1 + t_1\tilde{G}_H + t_2\tilde{G}_M + t_3\tilde{G}_H^2 + t_4\tilde{G}_H\tilde{G}_M + t_5\tilde{G}_M^2}, \tag{21}$$

$$S_H = \frac{s_4 + s_5\tilde{G}_H + s_6\tilde{G}_M}{1 + t_1\tilde{G}_H + t_2\tilde{G}_M + t_3\tilde{G}_H^2 + t_4\tilde{G}_H\tilde{G}_M + t_5\tilde{G}_M^2}. \tag{22}$$

The empirical parameters are listed in Table 3. These stability functions should be used together with the following realisability constraint (personal communication Vittorio Canuto)

$$G_H^{\lim} = 0.0673. \tag{23}$$

For a limitation of G_M, see Section 4.

In contrast to the stability functions of Mellor and Yamada (1982) and Kantha and Clayson (1994), the new stability functions are symmetric in two ways:

- Eddy viscosity and eddy diffusivity are calculated as functions of structurally the same combination of mean flow parameters, with only different empirical parameters.
- For both stability functions, normalised shear G_M and normalised stratification G_H occur symmetrically.
  This is an interesting feature of the Canuto et al. (2000) stability functions. However, the need for such a symmetry is matter of controversial scientific discussion, since momentum is in contrast to tracers additionally transferred by pressure fluctuations (personal communication Lakshmi H. Kantha).

4. Investigating normalised stresses

In a boundary layer, the shear stress $\tau = K_M S$, may be normalised as follows:

$$\frac{\tau}{q^2} = S_M G_M^{1/2}. \tag{24}$$

The normalised stress is fixed at the surface to $\tau/q^2 = \beta_1^{-2/3} \approx 0.15$ and vanishes at the stress-free bed. Due to the continuity of the flow, τ/q^2 has to adopt all values in between at certain depths.

This normalised stress may be readily plotted from the right-hand side of (24) for the Mellor and Yamada (1982) stability functions, see Fig. 2. It can be seen that the derivative of the normalised stress with respect to G_M is not monotone. This means that for fixed G_H more than one value of G_M leads to the same value for the normalised stress. It can further be seen that the line of bifurcation points is below the equilibrium line $P_s + P_b = \varepsilon$ such that the normalised stress τ/q^2 decreases there with normalised shear G_M.

In order to avoid this, $G_M^{\lim}$ has to be modified such that

$$\partial_{G_M} S_M G_M^{1/2} \geqslant 0. \tag{25}$$

Condition (25) is equivalent to

$$G_M^{\lim} = \frac{1 + b_1 G_H + b_3 G_H^2}{b_2 + b_4 G_H}. \tag{26}$$

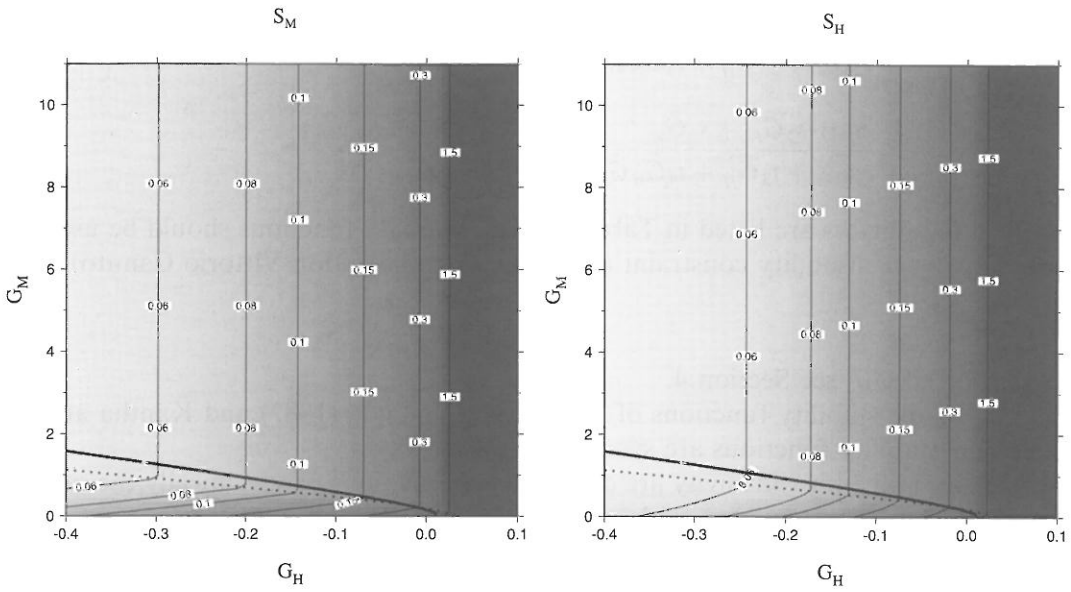

Fig. 2. Same as in Fig. 1, but with the constraint on G_M from Eq. (26), see dotted line.

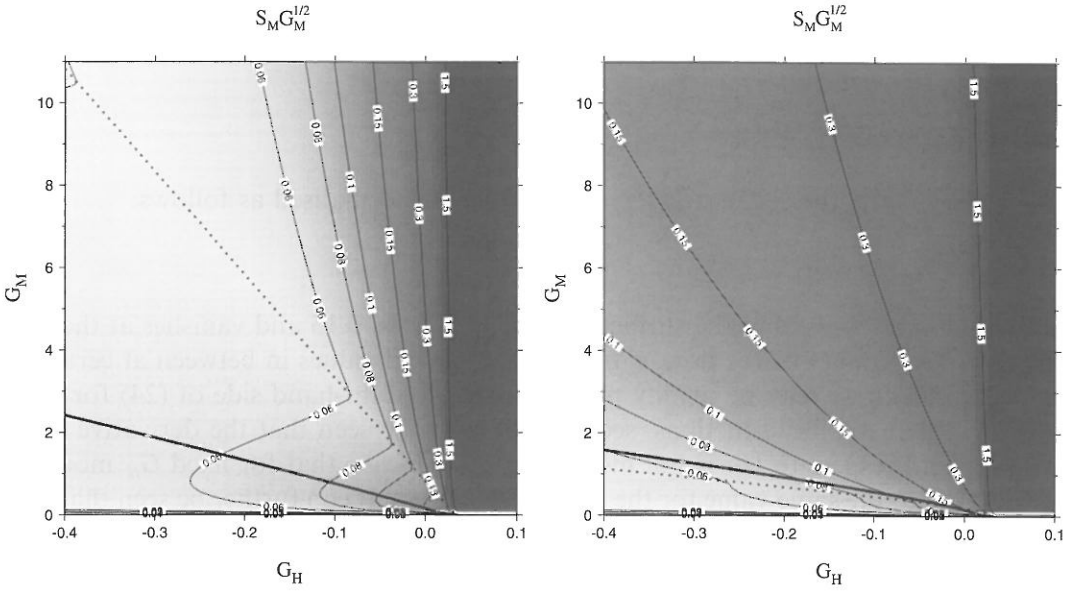

Fig. 3. The normalised shear stress as functions of G_M and G_H computed by using the Mellor and Yamada (1982) stability functions. Left: with constraint (19), right: with constraint (26), see dotted lines.

In Fig. 3, the normalised stress with the new constraint for G_M is shown. It can be seen that the curve for local equilibrium, $P_s + P_b = \varepsilon$ indeed lies fully outside this new constraint for G_M. It should be expected that using (26) instead of (19) would lead to a more stable performance of the

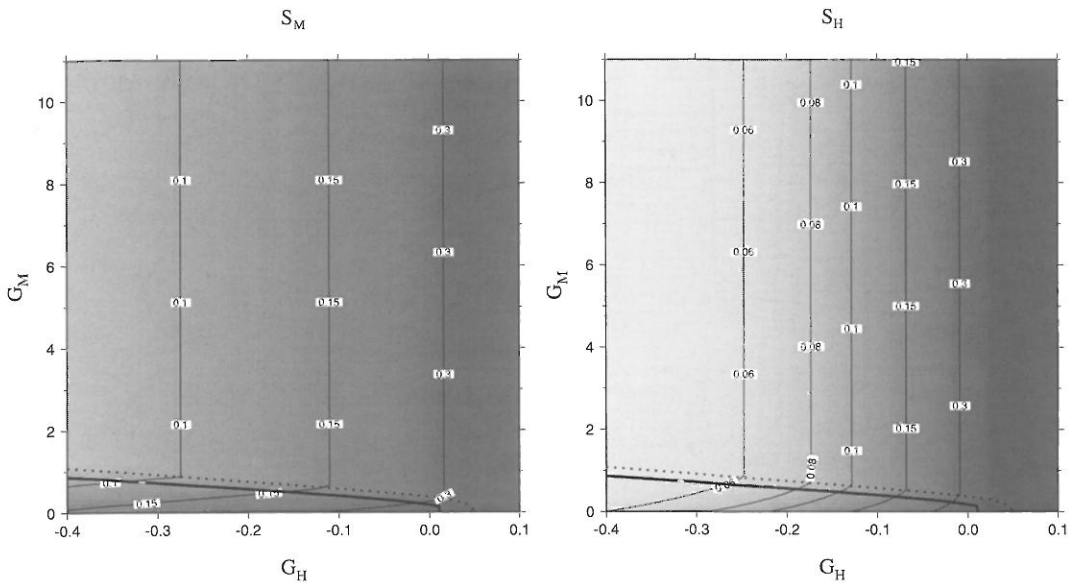

Fig. 4. The stability functions S_M and S_H as derived by Canuto et al. (2000). The bold lines show the local equilibrium state (20), the dotted lines show the constraint (27) on G_M with $\alpha = 1$.

complete model. This will be investigated in the next section by means of an idealised wind entrainment experiment.

For the model of Canuto et al. (2000), a similar constraint for G_M can be derived, if the terms with the small empirical parameters s_2 and t_5 are neglected (personal communication Vittorio Canuto)

$$G_M^{\lim} = \alpha \frac{1 + t_1 G_H + t_3 G_H^2}{t_2 + t_4 G_H} \tag{27}$$

For $\alpha = 1$, the Canuto et al. (2000) stability functions S_M and S_H are displayed in Fig. 4. In this case, (27) roughly ensures that the normalised stress is an increasing function of G_M, see Fig. 6. In contrast to the Mellor and Yamada (1982) model, the equilibrium state now lies fully below the monotonicity constraint (27). Since also larger values of α allow for stable simulations for the surface mixed layer, see Section 5, the Canuto et al. (2000) stability functions are also shown for $\alpha = 10$, see Fig. 5. In that case, of course, monotonicity of the normalised stresses is not any more given, see Fig. 6.

5. Wind entrainment experiment

An idealised wind entrainment experiment is used here in order to investigate the performance of the stability functions discussed in the previous section. The experiment carried out here is inspired by the laboratory experiment of Kato and Phillips (1969). In this experiment, a mixed layer induced by a constant surface stress penetrates into a stably stratified fluid with density

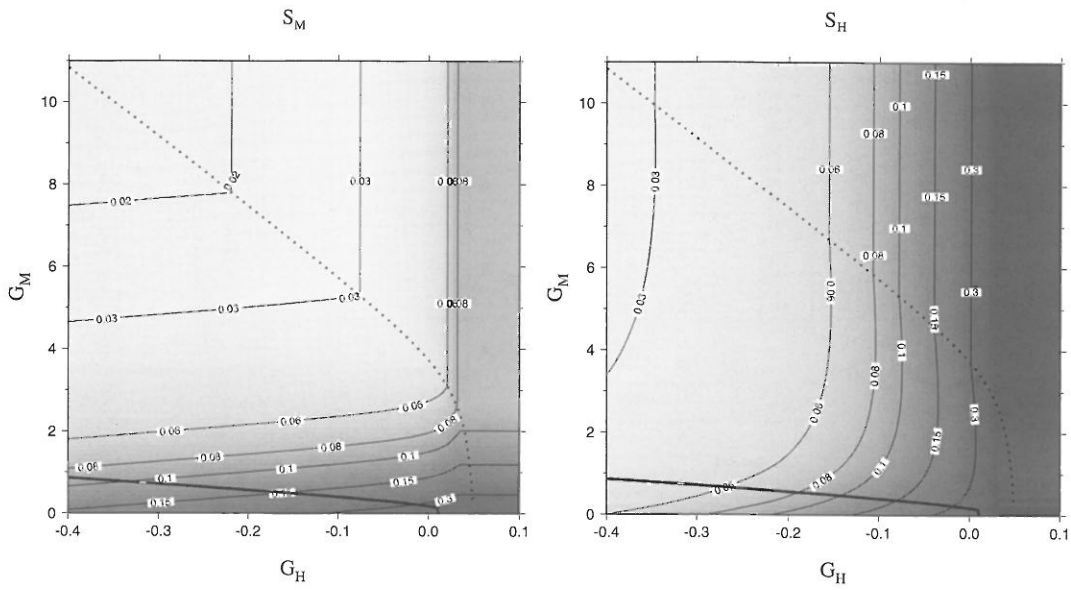

Fig. 5. The stability functions S_M and S_H as derived by Canuto et al. (2000). The bold lines show the local equilibrium state (20), the dotted lines show the constraint (27) on G_M with $\alpha = 10$.

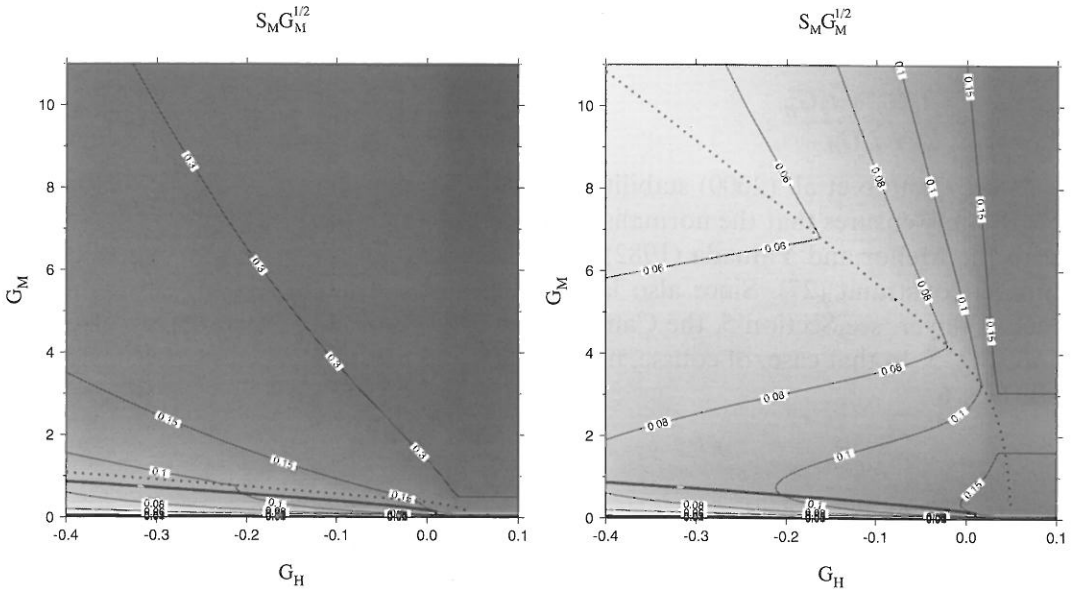

Fig. 6. The normalised shear stress as functions of G_M and G_H computed by using the Canuto et al. (2000) stability functions. The bold lines shows the local equilibrium state (20). The dotted lines show the constraint (27) on G_M: left: $\alpha = 1$; right: $\alpha = 10$.

increasing linearly down from the surface. The water depth is assumed to be infinite. Price (1979) suggested an empirical solution for the evolution of the mixed-layer depth D,

$$D(t) = 1.05\frac{u_*}{\sqrt{N_0}}t^{1/2}, \tag{28}$$

where N_0 is the constant initial Brunt-Väisälä frequency. Following Deleersnijder and Luyten (1994), we transform this laboratory experiment to ocean dimensions with $u_* = 10^{-2}$ m s^{-1} and $N_0 = 10^{-2}$ s^{-1}. The simulation will be run for 30 h, such that the empirical solution for the mixed-layer depth results in approximately 34.5 m.

The following numerical simulations of this wind entrainment experiment are carried out here:

1. Mellor and Yamada (1982) stability functions with the old constraint (19) on G_M and the q^2–q^2l model.
2. Mellor and Yamada (1982) stability functions with the old constraint (19) on G_M and the k–ε model.
3. Mellor and Yamada (1982) stability functions with the new constraint (26) on G_M and the q^2–q^2l model.
4. Mellor and Yamada (1982) stability functions with the new constraint (26) on G_M and the k–ε model.

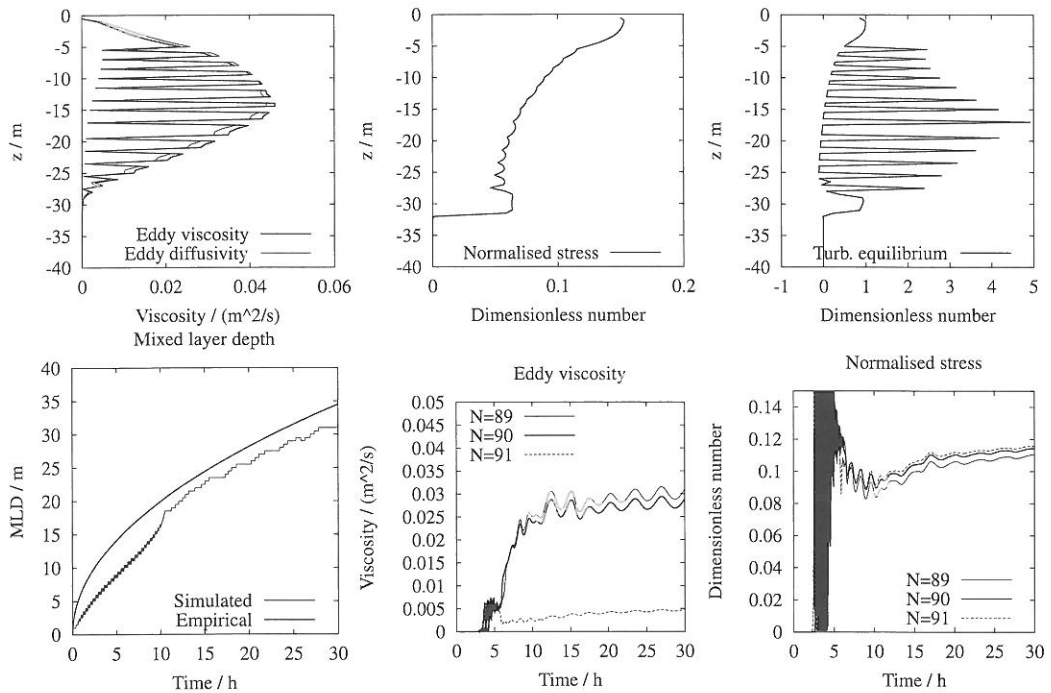

Fig. 7. Simulation results of run # 1 for the wind entrainment experiment by using the Mellor and Yamada (1982) stability functions with constraint (19) on G_M. The turbulent length scale is here calculated with the q^2l-equation (6). Shown are vertical profiles of eddy viscosity and diffusivity, normalised stress, and turbulence equilibrium $(P_s + P_b)/\varepsilon$. Furthermore, times series of eddy viscosity and normalised stress for three discrete points near the surface are shown.

5. Canuto et al. (2000) stability functions with the constraint (27) on G_M with $\alpha = 10$ and the k–ε model.

The time step is $\Delta t = 100$ s, and the vertical spacing is 0.5 m for all model runs. The discretisation is semi-implicit in time for the diffusion operator, the sink terms are discretised with the quasi-implicit method of Patankar (1980) in order to guarantee positivity of q^2, $q^2 l$ and ε. For further numerical details, see Burchard et al. (1999). For all model runs, profiles after 30 h for eddy viscosity and diffusivity, normalised stresses and turbulence equilibrium $(P_s + P_b)/\varepsilon$, and time series of mixed layer depth, eddy viscosity and normalised stress are shown in Figs. 7–11.

For both, the q^2–$q^2 l$ and the k–ε model, the stability functions by Mellor and Yamada (1982) with the original constraint on G_M, see Eq. (19), show significant spikes in the eddy viscosity and diffusivity profiles. This has already been shown by Deleersnijder and Luyten (1994) for the q^2–$q^2 l$ model. Similar spikes are visible for the turbulence equilibrium profiles. It is striking that except for the boundaries of the mixed layer, the expected value of $(P_s + P_b)/\varepsilon = 1$ is never close to unity. In contrast to that, the profiles of normalised stresses are rather smooth, with small spikes only. The same can be observed for the turbulent kinetic energy $q^2/2$ and the shear stress τ. This means that two solutions for the viscosity (and the shear) lead to the same shear stress, both of which are physically irrelevant, since they are far from the turbulence equilibrium. The time series of viscosity at three adjacent grid points about 5 m below the surface show that there are some oscillations in time with a period of the order of hours, much longer than the time step. The solution seems to be smooth in the beginning, but at a certain point, a bifurcation for the viscosities sets on

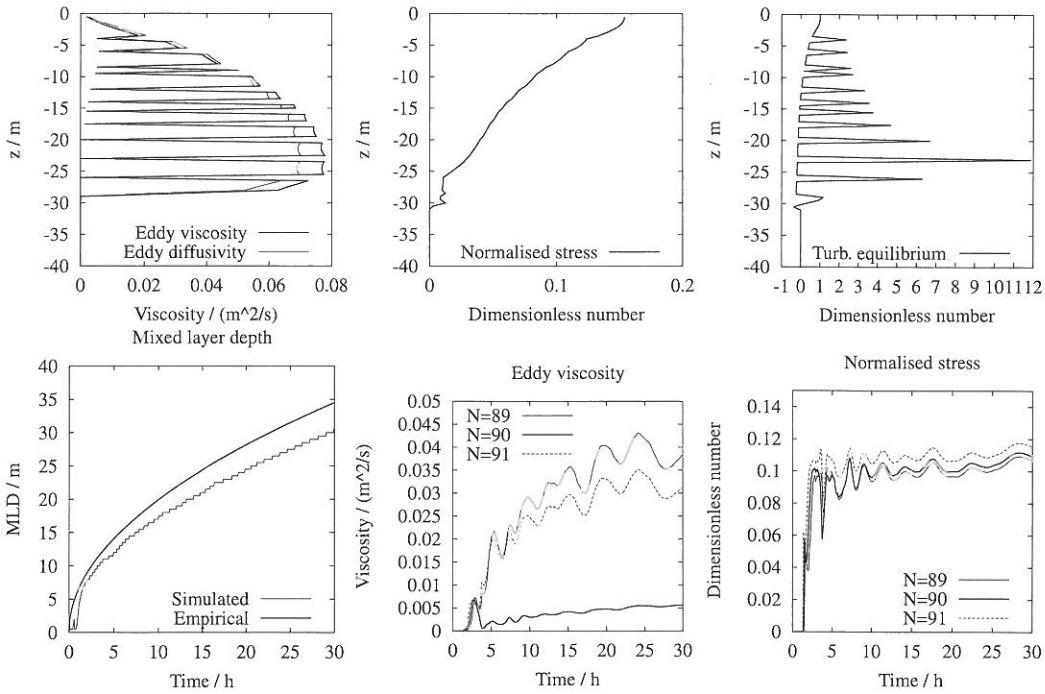

Fig. 8. Simulation results of run # 2 for the wind entrainment experiment by using the Mellor and Yamada (1982) stability functions with constraint (19) on G_M. The turbulent length scale is here calculated with the ε-equation (10).

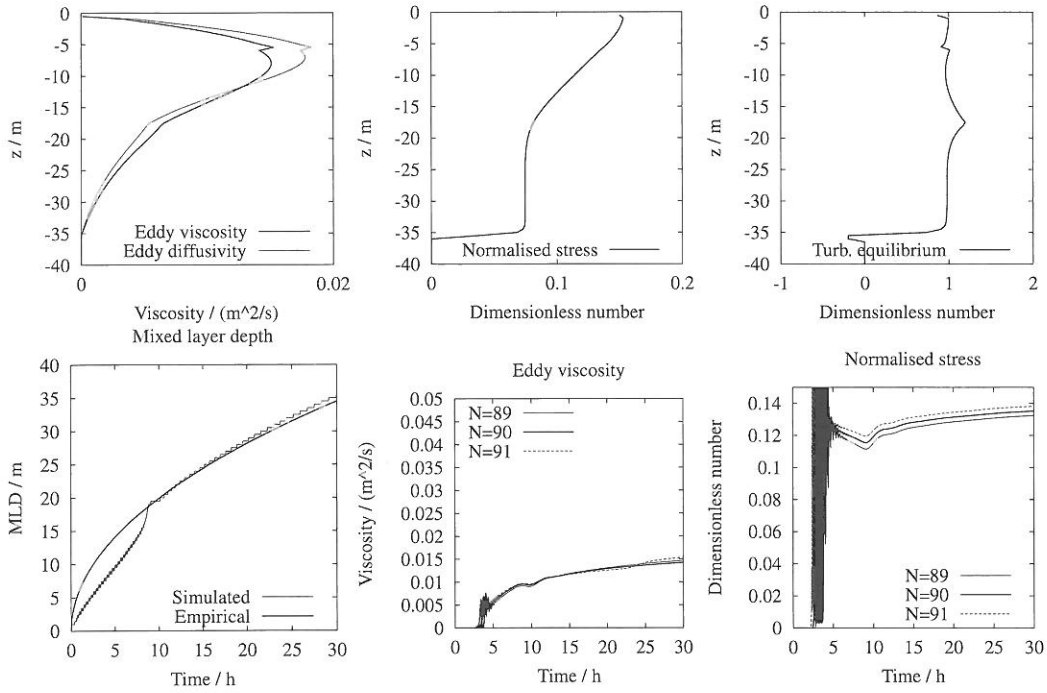

Fig. 9. Simulation results of run # 3 for the wind entrainment experiment by using the Mellor and Yamada (1982) stability functions with constraint (26) on G_M. The turbulent length scale is here calculated with the q^2l-equation (6).

(after about 3 h). The k–ε model performs numerically more stable, in contrast to the q^2–q^2l model which exhibits strong oscillations during the first 6 h after the sudden onset of surface stress. For both models, the empirical mixed layer depth is underestimated by a few meters.

When using the new constraint (26) instead of the original constraint (19), the bifurcation problem does not arise any more, and consequently, all profiles are rather smooth, for both the q^2–q^2l and the k–ε model. Only a small spike remains for the viscosity/diffusivity profiles which can be removed by further decreasing $G_M^{\lim}$. At about $z = -20$ m, an edge is visible for the eddy viscosity/diffusivity profiles, below which the q^2l equation is replaced by the length limitation (8). For further discussion of this feature, see Burchard (2001). Since for both models, turbulence is close to equilibrium over the whole mixed layer, it is not the original stability functions which are used here, but only the constraint (26). Both models show now a good agreement with the empirical mixed layer depth, although the results for the q^2–q^2l model still heavily oscillate during the first hours of simulation. These instabilities can be damped out by using smaller time steps.

So far, the results are consistent with the expectation that monotonic behaviour of normalised stresses with respect to G_M would avoid the bifurcation problem.

However, an inspection of the results obtained with the Canuto et al. (2000) stability functions contradicts this. As Fig. 11 demonstrates, results are stable even if the monotonicity constraint is strongly violated by setting $\alpha = 10$ in (27).

The differences of the results for $\alpha = 1$ and $\alpha = 10$ are small and only visible near the boundaries of the mixed layer. Values much larger than $\alpha = 10$ are not possible since then

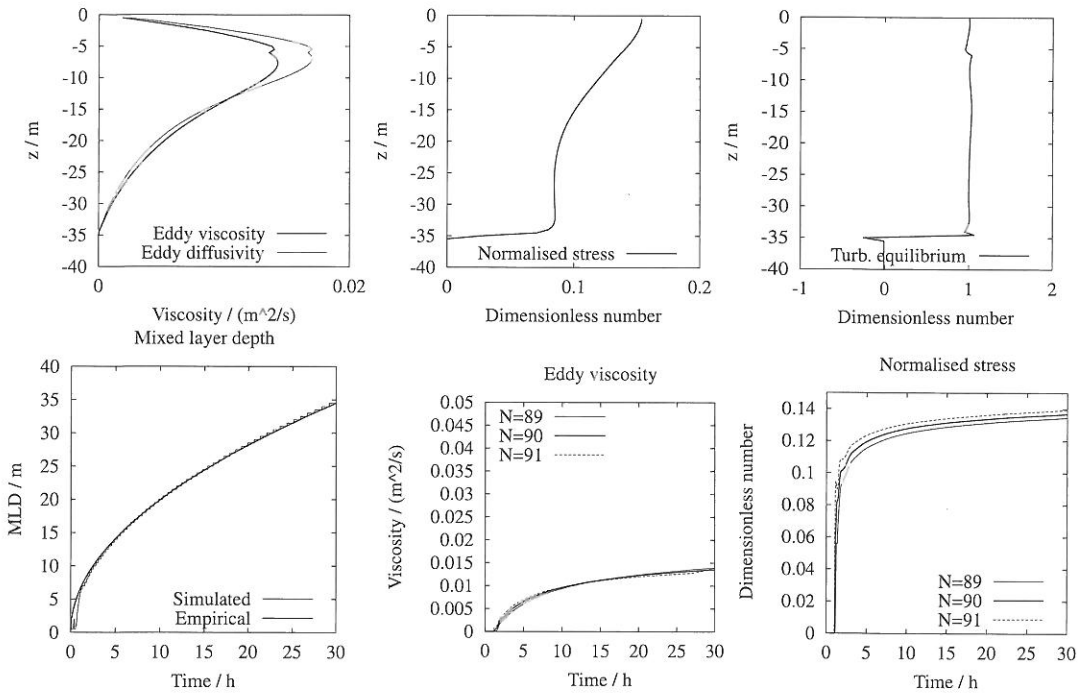

Fig. 10. Simulation results of run # 4 for the wind entrainment experiment by using the Mellor and Yamada (1982) stability functions with constraint (26) on G_M. The turbulent length scale is here calculated with the ε-equation (10).

negative values for the stability functions would be computed. The reason for the only small differences between the cases for $\alpha = 1$ and $\alpha = 10$ is, that for both cases, the equilibrium state $(P_s + P_b)/\varepsilon = 1$ is below the constraint on G_M. Since $(P_s + P_b)/\varepsilon \leqslant 1$ over the whole water column, this has the consequence that the normalised stresses everywhere increase with increasing shear.

Finally, the implications of five different sets of stability functions on mixing are demonstrated in Fig. 12, both, for the k–ε and the q^2–$q^2 l$ model. The following observations can be made:

- The quasi-equilibrium functions by Galperin et al. (1988) and by Kantha and Clayson (1994) compute only slightly different results due to the fact that only a few model parameters are changed, see Section 3.1.
- The stability functions by Mellor and Yamada (1982), modified by the constraint (26) are in some regions close to their quasi-equilibrium version, the Kantha and Clayson (1994) model, because the same empirical constants are used. However, in the region of strongest mixing significant differences occur due to the limitation Eq. (25) on G_M.
- The non-equilibrium and the quasi-equilibrium versions of the Canuto et al. (2000) stability functions are basically identical which is due to the TKE balance in the mixed layer. Only for the q^2–$q^2 l$ model, strong oscillations occur at the base of the mixed layer. A careful analysis proves that these are caused by the length scale limitation (8) which has to be used in the q^2–$q^2 l$ model. Burchard (2001) has recently shown that this length scale limitation can be avoided if much larger values for the empirical parameter E_3 are chosen for stable stratification. This increase of E_3 to a value of about 5 results in a macro length scale l which is equivalent to the

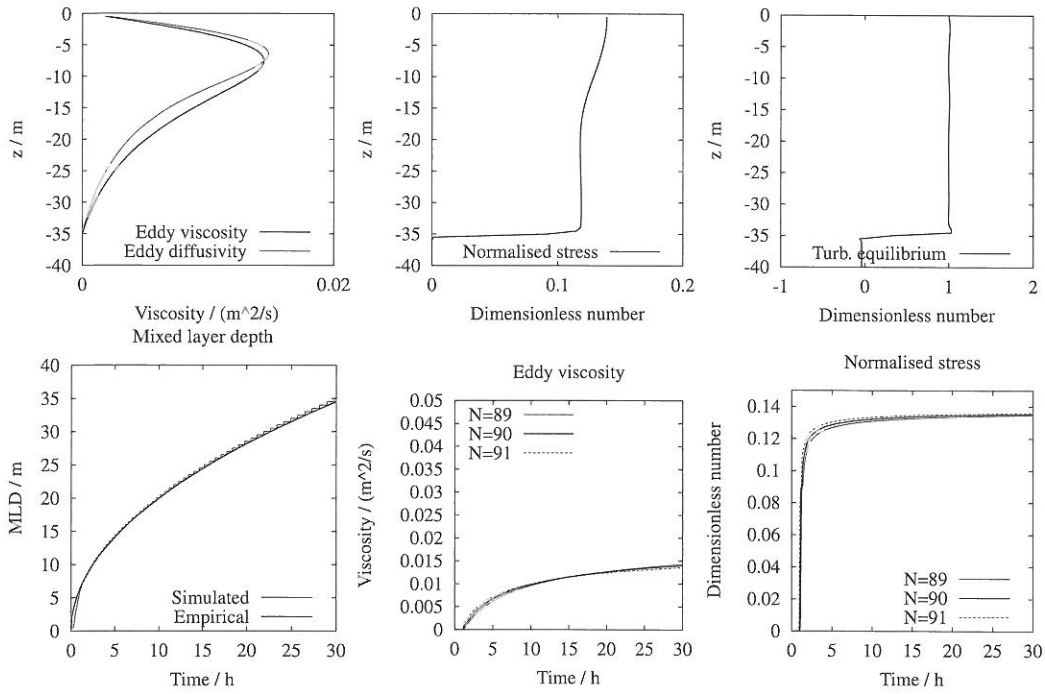

Fig. 11. Simulation results of run # 5 for the wind entrainment experiment by using the Canuto et al. (2000) stability functions with constraint (27) on G_M with $\alpha = 10$. The turbulent length scale is here calculated with the ε-equation (10).

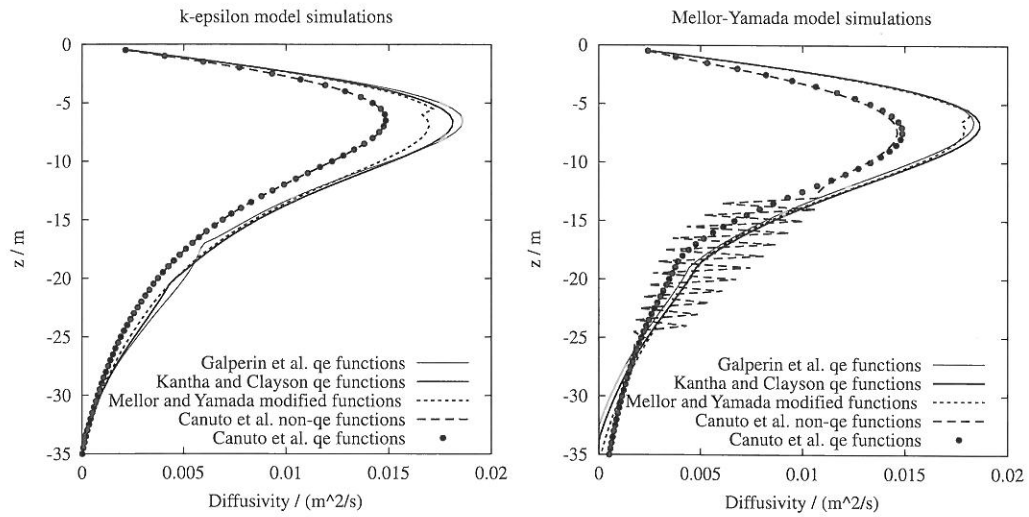

Fig. 12. Profiles of eddy diffusivity after 30 h of wind entrainment simulated with the k–ε model (left panel) and with the q^2–$q^2 l$ model (right panel) using different sets of stability functions, which are the Galperin et al. (1988) and the Kantha and Clayson (1994) quasi-equilibrium stability functions, the Mellor and Yamada (1982) stability function with modified constraint (26), and the full and the quasi-equilibrium versions of the Canuto et al. (2000) stability functions.

length scale from (8), if turbulence is in equilibrium, see Burchard (2001). After these physically motivated modifications, all oscillations vanish.

6. Discussion and conclusions

The persistent bifurcation problem of the Mellor and Yamada (1982) stability functions (with the Kantha and Clayson (1994) modification of the empirical parameters) could be demonstrated by means of using two different two-equation models, the q^2–$q^2 l$ and the k–ε model. This confirms the findings of Deleersnijder and Luyten (1994), who used the original Mellor and Yamada (1982) version for their investigation. This clearly shows that these stability functions are not at all useful neither in their original nor in the modified form. In some numerical models, these instabilities have been damped out by applying a Laplacian filter on the normalised shear G_M, see Pacanowsky et al. (1991). However, this manipulation proves not to work for high-resolution one-dimensional models. As shown in the present paper, it seems to be a solution of the problem to constrain the stability functions such that for increasing shear, the normalised shear stress does not decrease. This however has the consequence that the turbulence equilibrium state, which is closely approximated inside the mixed layer here, lies fully outside this new constraint, i.e., the constraint is always applied. This, of course, is a strong argument for using the quasi-equilibrium versions suggested by Galperin et al. (1988) and Kantha and Clayson (1994), in which the shear dependence of the stability functions is eliminated by inserting the turbulence equilibrium condition (20). Deleersnijder and Luyten (1994) could demonstrate the physically sound behaviour for the Galperin et al. (1988) stability functions. On the other hand, the quasi-equilibrium approximation is an assumption which disregards the additional physical information contained in a non-equilibrium algebraic second-moment turbulence closure. These advantages will be the more important, the more the flow is out of equilibrium, for example in situations of strong acceleration or in the entrainment region below a convective boundary layer. Thus, there are good arguments for constructing non-equilibrium algebraic second-moment turbulence closures which allow for stable numerical calculations. However, there are relevant processes in the ocean such as deep convection which cannot be reproduced in detail by the non-equilibrium models discussed here.

In contrast to the Mellor and Yamada (1982) stability functions, the Canuto et al. (2000) stability functions provide stable numerical calculations. This is obviously connected to the fact that the equilibrium state of turbulence, $(P_s + P_b)/\varepsilon = 1$ lies in a region where normalised shear stress increases with normalised shear, see Fig. 6. For the Mellor and Yamada (1982) stability functions, just the opposite happens: For turbulence equilibrium, normalised shear stress decreases with normalised shear, see Fig. 3. This physically more sound behaviour of the Canuto et al. (2000) stability functions is due to the higher number of terms considered for the parameterisation of the pressure–strain correlations (see also Canuto, 1994) with the additional consequence of symmetric stability functions and a significantly higher critical Richardson number.

It is obvious from Fig. 12 that the q^2–$q^2 l$ model computes less stable results than the k–ε model. This could be caused by the way how this model is numerically discretised here. However, the fact that all oscillations vanish after replacing the length scale limitation (8) by a physically motivated increase of the empirical parameter E_3 for stable stratification, see Burchard (2001), suggests that this limitation is responsible for the instabilities. It should be noted that this modification has

already been suggested by in 1988 by Lakshmi H. Kantha in an unpublished manuscript (On some aspects and applications of second-moment closure, Atmospheric and Oceanic Sciences Program, Princeton University, 167 pp., 1988). This approach has however not been further followed by Lakshmi H. Kantha and co-workers, perhaps because of the acceptable performance of the original, unmodified version with length scale limitation instead of a higher value for E_3.

Acknowledgements

The work of Hans Burchard has been funded through a Habilitation grant by the Deutsche Forschungsgemeinschaft (German Research Foundation) and the project PROVESS (MAS3-CT97-0025) of the MAST-III program of the European Commission. Eric Deleersnijder is a Research Associate with the National Fund for Scientific Research of Belgium. The authors are indebted to Vittorio Canuto (New York) and Lakshmi Kantha (Boulder) for constructive criticism of a previous version of the manuscript. All numerical model calculations for this paper have been carried out by using the Public-Domain water column model GOTM (General Ocean Turbulence Model, see on the World Wide Web at http://www.gotm.net).

References

Blumberg, A.F., Mellor, G.L., 1987. A description of a coastal ocean circulation model. In: Heaps, N.S. (Ed.), Three dimensional ocean models. American Geophysical Union, Washington, DC, pp. 1–16.

Burchard, H., 2001. Note on the q^2l equation by Mellor and Yamada (1982). Journal of Physical Oceanography, in press.

Burchard, H., Bolding, K., 2000. Comparative analysis of four second-moment turbulence closure models for the oceanic mixed layer. Journal of Physical Oceanography, accepted for publication.

Burchard, H., Bolding, K., Villarreal, M.R., 1999. GOTM – a general ocean turbulence model. Theory, applications and test cases. Report EUR 18745 EN, European Commission, p. 103.

Canuto, V.M., 1994. Large eddy simulation of turbulence: a subgrid model including shear, vorticity, rotation and buoyancy. Journal of Astrophysics 428, 729–752.

Canuto, V.M., Howard, A., Cheng, Y., Dubovikov, M.S., 2000. Ocean turbulence I: one-point closure model. Momentum and heat vertical diffusivities with and without rotation. Journal of Physical Oceanography, accepted for publication.

Deleersnijder, E., Luyten, P., 1994. On the practical advantages of the quasi-equilibrium version of the Mellor and Yamada level 2.5 turbulence closure applied to marine modelling. Applied Mathematical Modelling 18, 281–287.

Galperin, B., Kantha, L.H., Hassid, S., Rosati, A., 1988. A quasi-equilibrium turbulent energy model for geophysical flows. Journal of Atmospheric Sciences 45, 55–62.

Kantha, L.H., Clayson, C.A., 1994. An improved mixed layer model for geophysical applications. Journal of Geophysical Research 99, 25235–25266.

Kato, H., Phillips, O.M., 1969. On the penetration of a turbulent layer into stratified fluid. Journal of Fluid Mechanics 37, 643–655.

Martin, P.J., 1985. Simulation of the mixed layer at OWS November and Papa with several models. Journal of Geophysical Research 90, 903–916.

Mellor, G.L., 2001. One-dimensional, ocean surface layer modeling, a problem and a solution. Journal of Physical Oceanography 31, 790–809.

Mellor, G.L., Yamada, T., 1974. A hierarchy of turbulence closure models for planetary boundary layers. Journal of Atmospheric Sciences 31, 1791–1806.

Mellor, G.L., Yamada, T., 1982. Development of a turbulence closure model for geophysical fluid problems. Reviews of Geophysics 20, 851–875.

Pacanowsky, R., Dixon, K., Rosati, A., 1991. README file for GFDL MOM 1.0, GFDL/NOAA, Princeton, New Jersey.

Patankar, S.V., 1980. Numerical Heat Transfer and Fluid Flow. McGraw-Hill, New York.

Price, J.F., 1979. On the scaling of stress-driven entrainment experiments. Journal of Fluid Mechanics 90, 509–529.

Rosati, A., Miyakoda, K., 1988. A general circulation model for upper ocean simulation. Journal of Physical Oceanography 18, 1601–1626.